Journal of Applied Polymer Science

Numerical simulation of flow of rubber compounds in partially filled internal mixer

Jinpeng Liu,[1] Fanzhu Li,[2] Liqun Zhang,[1] Haibo Yang[1]

[1]Key Laboratory of Beijing City on Preparation and Processing of Novel Polymer Materials, Beijing University of Chemical Technology, Beijing 100029, China

[2]State Key Laboratory of Organic-Inorganic Composites, Beijing University of Chemical Technology, Beijing 100029, China

Correspondence to: H. Yang (E-mail: yanghb@mail.buct.edu.cn)

ABSTRACT: Most numerical simulations of the flow in an internal mixer are based on the assumption that the internal mixer is totally filled with rubber compounds. However, in fact, the internal mixers are only partially filled with rubber compounds, thus posing many challenges for researchers in simulating the flow in the internal mixer. In this study, the volume of fluid method and the dynamic mesh technology of commercial CFD software FLUENT were used to simulate the flow of rubber compound in a partially filled internal mixer. To improve simulation accuracy, every 18 degrees in circumferential direction, we manually re-meshed the calculated transient location of the rubber compound. Thus, we obtained the transient distribution of the rubber compound in the internal mixer as the rotors rotated. The simulation results showed that voids were mainly located behind the rotor blades, and there were material exchanges in the bridge regions between the two chambers. © 2015 Wiley Periodicals, Inc. J. Appl. Polym. Sci. **2015**, *132*, 42496.

KEYWORDS: blends; rubber; theory and modelling

Received 3 February 2015; accepted 12 May 2015

DOI: 10.1002/app.42496

INTRODUCTION

Internal mixers are widely applied in the rubber industry to mix rubbers with carbon black and other ingredients to produce composites with desirable properties.[1,2] The mixing efficiency of an internal mixer directly depends on the flow characteristics in the mixing chamber, whereas the flow characteristics in the mixing chamber are related to the rotor geometry and the operational parameters such as fill factor, temperature, rotor speed, and duration of the mixing cycle. To improve the mixing efficiency of the internal mixer, the flow characteristics in the mixing chamber and the relations between the rotor geometry, the operational parameters, and the flow characteristics in the mixing chamber must be well studied. However, to the best of our knowledge, such studies on the flow characteristics in the mixing chamber are far from sufficient.

So far many researchers have used experiments to study the flow characteristics in internal mixers. Published experimental studies on the internal mixer primarily involved measurements of energy input, torque, pressure, and temperature history at fixed positions.[3] The degree of mixing was usually characterized by measuring the agglomerate size of fillers at various mixing times by a scanning electron microscope.[4,5] For example, Freakley and Patel[6] used the results of mixing trials with a highly instrumented Banbury mixer to examine the influence of fill factor, rotor speed, and mixing time on the temperature and pressure generated in the rubber compound. But these experimental approaches cannot determine how the rubber compounds flow in an internal mixer. Understanding the flow in an internal mixer is the primary step to establish a physical model and then a mathematical model about the internal mixer. Flow visualization allows a direct observation of the mixing process and a better understanding of the flow in the mixing chamber. This method was first reported by Freakley and Idris.[7] They used a miniature mixer with a transparent plastic chamber to observe the dynamics of the mixing of silicone rubber. Min and White[8,9] used a laboratory-scale mixer with glass front and transverse windows to investigate the flow of SBR, BR, and NR, and various molten plastics. Flow visualization gives important information about the mixing process, showing the flow patterns within the mixer. But flow visualization cannot provide such data as local velocities, pressures, shear rates, and shear stresses. In addition, this technique usually requires new rotor structures and some special equipment, and is generally expensive and time consuming. On the other hand, the flow simulation of mixing is of increasing interest to researchers due to recent performance increases in computer hardware and the availability of advanced software packages for complex flow simulation. Flow simulation can provide a fundamental understanding of the flow mechanics of an internal mixer and is a powerful tool for optimizing the rotor.

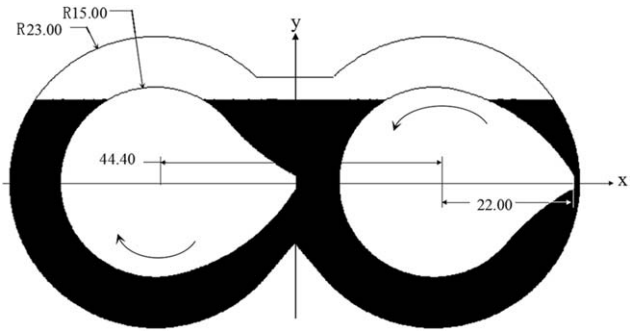

Figure 1. Geometric model and initial configuration of rubber compound in partially filled internal mixer.

A substantial amount of simulation work on internal mixer has been conducted by various researchers.[10–23] Bai and Sundararaj[10] studied the transient temperature development due to viscous dissipation inside an internal batch mixer, using 3D nonisothermal CFD modeling. Salahudeen *et al.*[14] performed simulation work on an miniature internal mixer to compare the mixing efficiency of various rotor geometries such as cam, Banbury rotors, and roller. Ghoreishy and Nassehi[18] modeled the transient flow of rubber compounds in the dispersive section of an internal mixer with slip-stick boundary conditions. However, the above studies were all performed on the assumption that the internal mixers are totally filled with rubber compounds. In fact, for rubber mixing, the chamber of an internal mixer is only partially filled with rubber compound. The fill factor, which is defined as the ratio of the volume of the rubber compound to the total volume of the chamber, is an important parameter. The fill factor of an internal mixer suitable for the mixing of rubber is about 70–75% through experience.[3] Apparently the assumption of the totally rubber compound-filled condition in most simulations conflicts with the real partially rubber compound-filled mixing process in an internal mixer, and consequently, this assumption leads to the low accuracy of the numerical simulation. The purpose of the assumption of the totally filled condition is to avoid solving the free surface flow problem resulting from the partially filled condition. So far, the numerical analysis of mixing in partially filled internal mixers was only performed by Ghoreishy and Nassehi.[24,25] A combined Eulerian-Lagrangian approach was used to model the free surface flow in an internal mixer. The most interesting feature of the results was the appearance of a small vacuum region at the back of the rotor. In their studies, the location of the free surface corresponded to an element boundary, and the free surface captured was relatively rough. The method may be more accurate with a well-defined mesh. However, the method implemented in their studies is not robust when modeling free surfaces that merge, separate, or are convoluted. Overall, the understanding of the flow behaviors of rubber compounds in partially filled internal mixer is still far from satisfactory. In this study, we explored the issue of free surface flow in a partially filled mixer for a better understanding of the mixing process.

Numerical methods for solving the free surface flow problems can be divided into Lagrangian, mixed Eulerian-Lagrangian, and Eulerian methods.[26] The Eulerian approach, which makes use of a fixed mesh, does not involve high computational costs. Based on the Eulerian approach, the volume of fluid (VOF) method has been confirmed by numerical studies[27–35] to be well suited for solving free surface flow problems and to yield good predictions. This approach has been successfully used to model the broken dam problem,[28,34] trickle-bed reactor,[29] casting filling process,[30] and rotating packed bed reactor.[31]

In this study, the partially filled flow of rubber compound in an internal mixer was computed by using the VOF method and dynamic mesh technology of the commercial CFD software FLUENT. Because of the restriction of computer ability at present, the 3D simulations of internal mixer with free surface flow are time consuming. Therefore, the present simulation was limited to 2D. To improve simulation accuracy, every 18 degrees in circumferential direction, we manually re-meshed the calculated transient location of the rubber compound. Thus, we obtained the transient distribution of the rubber compounds in the internal mixer as the rotors rotated.

DESCRIPTION OF SIMULATION METHOD

The whole rubber compound mixing process in an internal mixer can be divided into five stages: the broken stage, the mixing stage, the dispersive stage, the distributive stage, and the plasticized stage. It is difficult to simulate the first four stages by CFD because solid mechanics and the interactions between the fillers and the rubber matrix must be included in such stages. In the last period of the fifth stage, rubber compound is plasticized and the flow of rubber compound is appropriate to be simulated by CFD. This article concentrates on simulating the flow of the plasticized rubber compound in the last period of the fifth stage using software FLUENT.

Finite Element Model

To simplify building the model, we assumed that at the initial time, the rubber compound (black region in Figure 1) was located in the lower part of the chamber in an internal mixer with two tangential rotors and the rest region (white region in Figure 1) of the chamber was full of air. The fill factor of the configuration was limited to 70–75% suitable for the mixing of rubber by adjusting the vertical location of the boundary line between the rubber compound and the air. In the article, the fill factor of the configuration is 73%. The model sizes are acquired from the XSM-500 internal mixer in our laboratory. The diameter of the chamber and the gap between the blade tip and the chamber wall is 46 and 1.0 mm, respectively. The center distance between the centers of the two rotors is 44.4 mm. The CFD preprocessor GAMBIT was used to define the boundaries and generate the meshes of the model. To guarantee calculation accuracy, a small value was assigned to the element size. The total numbers of elements and nodes for the initial geometry are 59,466 and 30,637, respectively.

The Cross model[36] was used to describe the rheological properties of the rubber compounds:

$$\eta = \frac{\eta_0}{1+(\lambda\dot{\gamma})^{1-n}} \tag{1}$$

where η_0 is the zero-shear viscosity, λ is a model parameter representative of relaxation time, and n is the Cross-law index.

Fitting eq. (1) to the experimental data for the rubber compound SSBR/N330, we obtained $\eta_0 = 21730$ Pa·s, $\lambda = 0.118$ s, and $n = 0.086$. The rubber compound was assumed to be incompressible, and with a density of 1100 kg/m^3. For air, the density and the viscosity of air were 1.225 kg/m^3 and 10^{-5} Pa·s, respectively.

As no-slip boundary condition is commonly used in CFD (computational fluid dynamics) and can meet the precision requirements in engineering, it is applied at the rotor surfaces and the chamber wall. Thus, the velocity of the fluid at the rotor surfaces is equal to the velocity of the rotors, and the velocity of the fluid at the chamber wall is set to zero. The two rotors counter rotate with an identical speed of 6.28 rad/s. Body forces are not included. It is reasonable to assume that the flow of the rubber compound is isothermal because the temperature of the rubber compound almost remains stable in the last period of the fifth stage. In addition to concentrate on overcoming the difficulty on the partially rubber compound–filled condition in the simulation, the isothermal flow assumption is reasonable and necessary. The simulation was performed by using the commercial CFD code FLUENT. The dynamic mesh method in FLUENT was used to model the moving rotors and account for the continuously varying flow domain as the rotors rotated by providing a starting volume mesh and a description of the rotation of the rotors with user-defined functions (UDFs).

VOF Model

The VOF model, proposed by Hirt and Nichols,[37] is based on the description of the volume fraction of each phase in element. The continuity equation for the volume fraction of the rubber compounds in the computational domain is expressed as:

$$\frac{\partial \alpha_r}{\partial t} + \nabla \cdot (\alpha_r \vec{v}_r) = 0 \quad (2)$$

where α_r is the volume fraction of the rubber compound in an element and $\vec{v}_r$is the velocity of the rubber compound. If an element is filled with the rubber compound, $\alpha_r = 1$, and if an element is filled with air, $\alpha_r = 0$. The free surface of the rubber compound can be considered to exist in the partially filled elements with α_r values between 0 and 1, usually 0.4–0.5.[38]

A single momentum equation is solved throughout the domain:

$$\frac{\partial}{\partial t}(\rho \vec{v}) + \nabla \cdot (\rho \vec{v} \vec{v}) = -\nabla p + \nabla \cdot \left[\mu(\nabla \vec{v} + \nabla \vec{v}^T)\right] + \vec{F}_v \quad (3)$$

where $\vec{v}$is the velocity vector, P is the pressure, ρ is the density, μ is the viscosity, and $\vec{F}_v$ is the body force. The physical properties in the governing flow equation are determined as follows:

$$\phi = \phi_r \alpha_r + \varphi_a (1\text{-}\alpha_r) \quad (4)$$

where ϕ is a physical parameter, ϕ_r and ϕ_a are the values of the physical parameter for the rubber compounds and air, respectively.

The solution starts from the initial distribution of the volume fraction values. At the end of each time step, new values of α_r are obtained and the position of the free surface of the rubber compounds is updated. However, because eq. (2) is solved numerically, the free surface becomes more and more indistinct as computation goes on due to the numerical false diffusion of α_r, even with a highly accurate integration of eq. (2). Therefore, we developed a solution strategy to solve the problem. The overall solution strategy is summarized as follows:

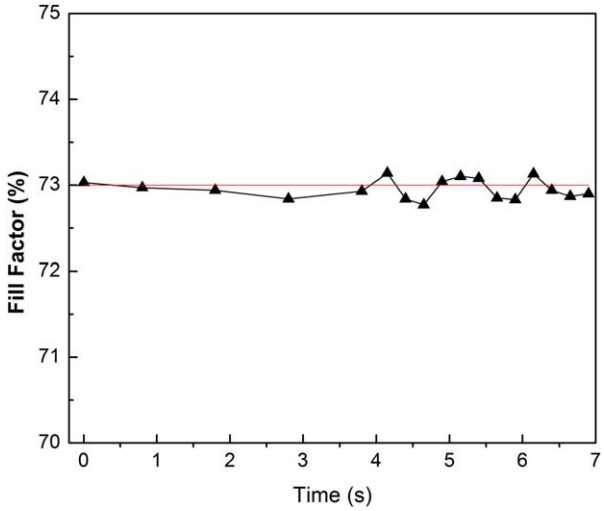

Figure 2. The variation of the fill factor with time. [Color figure can be viewed in the online issue, which is available at wileyonlinelibrary.com.]

1. Start from an initial configuration and divide the whole domain into meshes. The initial volume fraction of the rubber compound in each element is known.
2. Solve the governing equations by FLUENT in time steps of 10^{-6} s each for 50,000 steps and obtain values of α_r for every element at each new time.
3. Calculate the threshold value $\alpha_{r,s}$ to keep the volume of the rubber compound constant. The rubber compound completely fill an element whose volume fraction α_r is above the threshold value $\alpha_{r,s}$.
4. Assign the values of α_r above $\alpha_{r,s}$ to be 1, and the values of α_r below $\alpha_{r,s}$ to be 0. Export the volume fraction of each element.
5. Construct new finite element meshes from the distribution of rubber compound determined by the newly computed values of α_r and interpolate the new values of α_r to the new finite element meshes.
6. Repeat steps (2)–(5) until the final time is reached.

With the above solution strategy, a distinct free surface for the rubber compound was obtained, and the volume of the rubber compound was kept constant.

RESULTS AND DISCUSSION

At each new time during computation, the value of α_r (the volume fraction of the rubber compound) and the volume of each element are exported. Designate an initial threshold value of α_r as 0.5 and sum the volume of the elements with $\alpha_r \geq 0.5$ to obtain the value of V_r (the volume of the rubber compound), then divide V_r by the total volume of the chamber to obtain the fill factor. If the fill factor does not approximately equal to 0.73, change the threshold value of α_r and recalculate the fill factor using the same method above until the fill factor is approximately equal to 0.73.

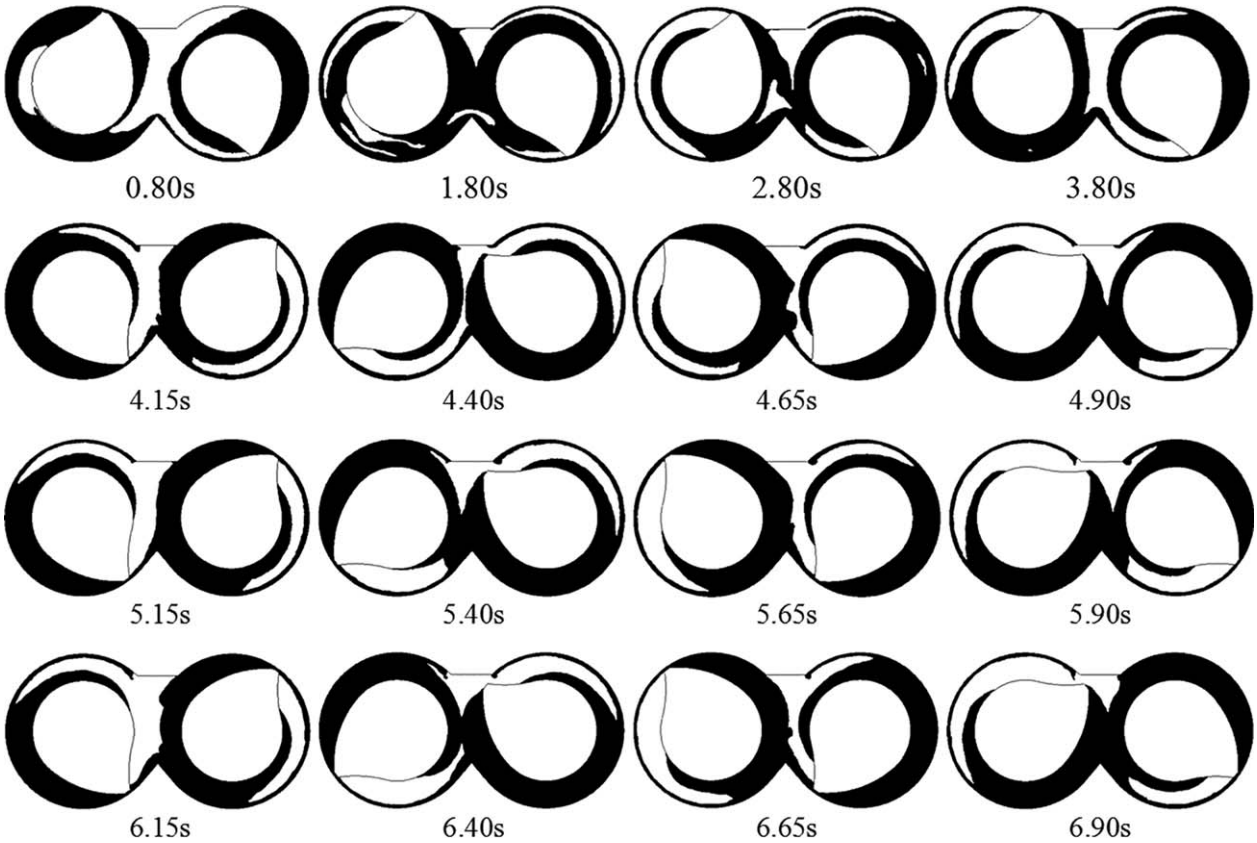

Figure 3. Distributions of rubber compound at consecutive times.

Figure 2 shows the value of the fill factor at the corresponding time points. The fill factor remains almost unchanged during the process of simulation. The maximum relative difference is 0.32%.

Simulated Material Distribution

Figure 3 shows the rubber compound distributions at consecutive times. After the rotors have rotated four times, the rubber compound distribution of the current turn will remain the same as that of the preceding turn. When the flow of the rubber compound is stable, they are mainly distributed in the regions in front of the rotor blades and the gap regions between the rotor blades and the inner wall of the mixing chamber, which are referred to as the high shear regions. Such rubber compound distributions imply that there are always rubber compound going through the high shear regions at the tips of the rotor blades. At the back of the rotor blades and below the ram, there is no rubber compound. A thin layer of the rubber compound is distributed on the inner wall of the mixing chamber.

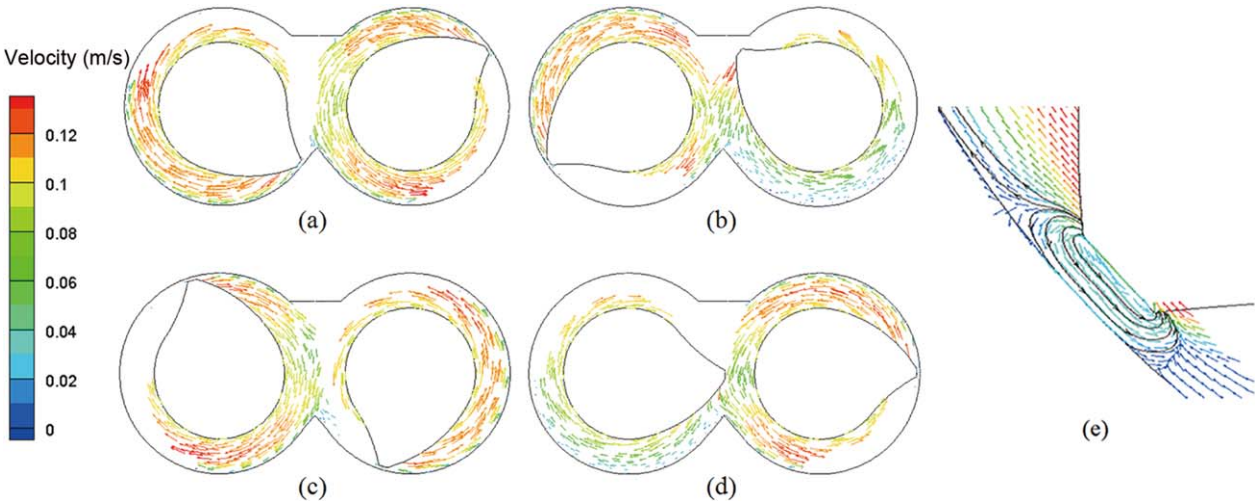

Figure 4. Distributions of velocity vectors at four sequential locations of the rotors in a cycle: (a) $\theta = 36°$, (b) $\theta = 144°$, (c) $\theta = 252°$, and (d) $\theta = 360°$. (e) The left rotor tip region. [Color figure can be viewed in the online issue, which is available at wileyonlinelibrary.com.]

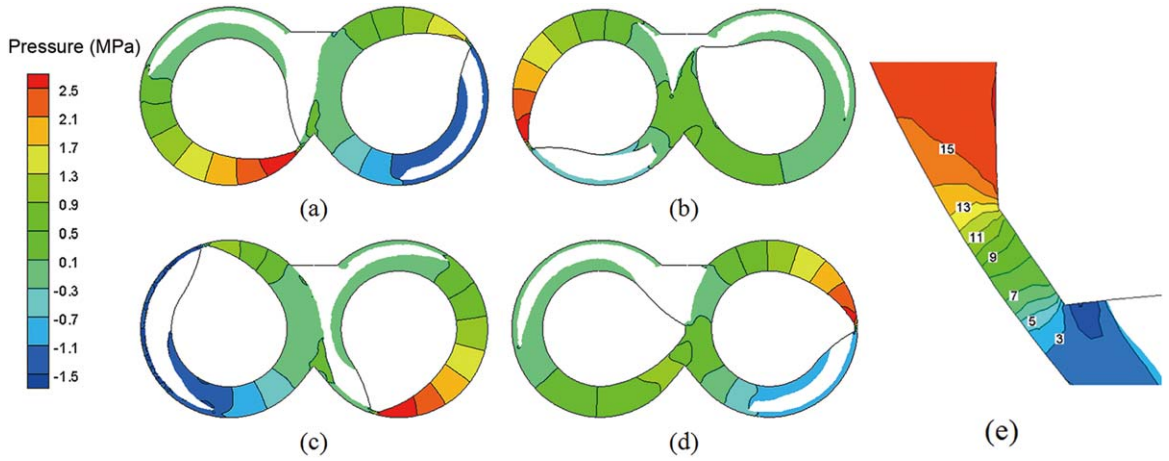

Figure 5. Pressure distributions of at four sequential locations of the rotors in a cycle: (a) $\theta = 36°$, (b) $\theta = 144°$, (c) $\theta = 252°$, (d) $\theta = 360°$. (e) The left rotor tip region. [Color figure can be viewed in the online issue, which is available at wileyonlinelibrary.com.]

This situation may be caused by applying the no-slip boundary condition.

Velocity Distribution

To analyze the flow characteristics, we select four sequential locations of the rotors in a cycle between 5.0 and 6.0 s because the rubber compound distribution remains unchanged from one cycle to the next cycle after the rotors rotate four times. The locations of the rotors are defined by the angle θ between the right blade tip and the X-axis.

From the velocity vector distribution shown in Figure 4, the rubber compound in the left and the right mixing chamber largely flow circularly, following the rotation of the rotors. In the bridge regions between the two rotors, the intersection of the velocity vectors implies that there is exchange of the rubber compounds between the left and the right mixing chamber. Furthermore, the exchange of the rubber compounds is more violent with the rotor tip inside the bridge region than with the rotor tip outside the bridge region. In the rotor tip region, the existence of velocity vector opposite to the rotation of the rotors implies that backflow takes place and the velocity gradient of this region is relatively large. The scatter of the velocity vectors around the blade tip corner indicates a kneading effect on the rubber compounds. The exchange of rubber compound in the bridge region, the backflow of rubber compounds, the relatively high shear rate in the rotor blade tip region, and the kneading effect on the rubber compounds are all beneficial to the mixing efficiency of the internal mixer.

Pressure Distribution

Figure 5 shows the pressure distributions at four sequential locations of the rotors in a cycle. The maximum pressure is

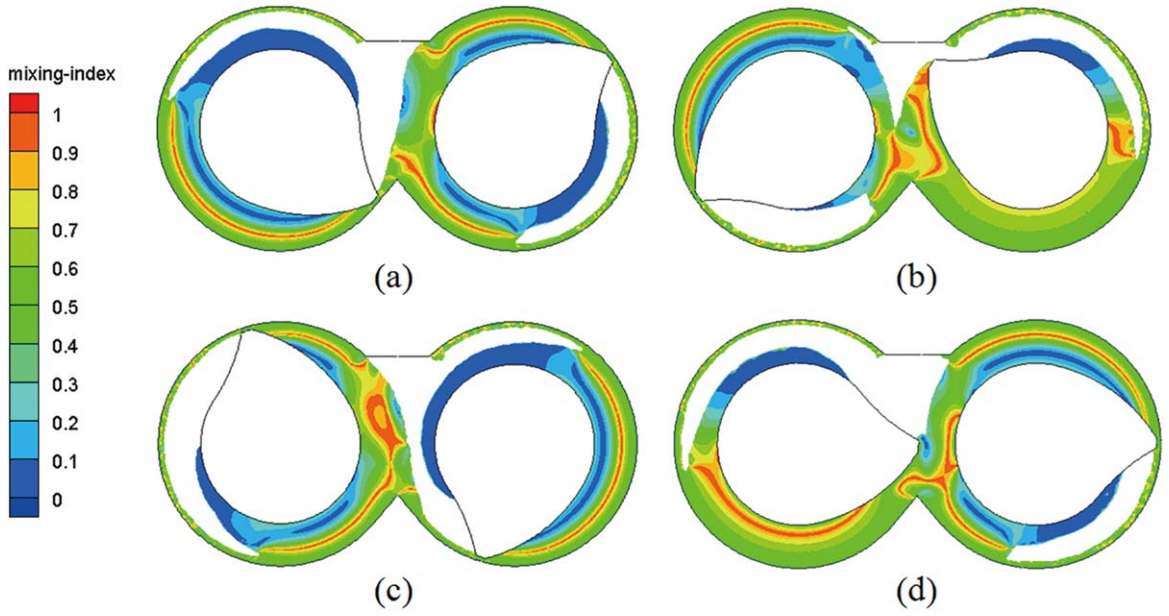

Figure 6. Mixing index distribution at four sequential locations of the rotors in a cycle: (a) $\theta = 36°$, (b) $\theta = 144°$, (c) $\theta = 252°$, and (d) $\theta = 360°$. [Color figure can be viewed in the online issue, which is available at wileyonlinelibrary.com.]

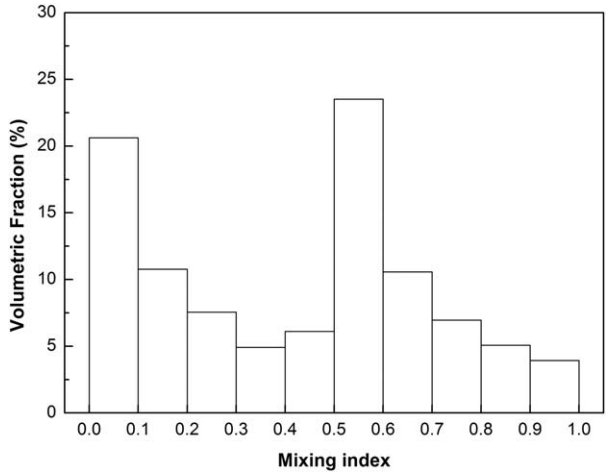

Figure 7. Volume distribution of λ_{MZ} at $\theta = 36°$.

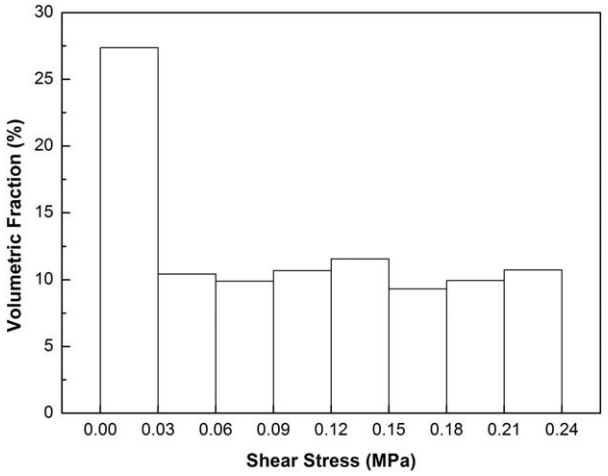

Figure 9. Volume distribution of shear stress at $\theta = 36°$.

located at the entry of the gap between the blade tip and chamber wall, and the high pressure causes a squeezing effect on the rubber compounds around the rotor blade tip corner. The pressure then decreases as the distance between the outlines of the rotor and the chamber wall increases until the pressure reaches a low and uniform value. The squeezing effect helps to disperse the filler added into the rubber matrix. The regions between the blade tip and chamber wall and around the rotor blade tip corner may be the main place where the dispersion takes place. The minimum pressure is located in the rear of the blade tip, in accordance with experimental observations.[6] A relatively large pressure gradient exists in the rotor blade tip region. However, the pressure gradient in the rotor blade tip region is strongly dependent on the relative positions of the rotors. There is a difference between the two rotors. The pressure gradient is larger with the rotor blade tip inside the left or the right mixing chamber than with the rotor blade tip inside the bridge region.

Dispersive Mixing

Because elongational flows are more effective for dispersion than simple shear flows, a mixing index (λ_{MZ}) is proposed by Manas-Zloczower[39] to measure the elongation flow and is defined as

$$\lambda_{MZ} = \frac{|D|}{|D| + |\Omega|} \tag{5}$$

where |D| and |Ω| are the magnitudes of the rate of deformation tensor and the vorticity tensor, respectively. λ_{MZ} varies between 0, for a pure rotational flow, to 1, for a pure elongational flow.

Figure 6 shows the mixing index distribution at four sequential locations of the rotors in a cycle. Rotational flow ($\lambda_{MZ} < 0.2$) dominates the regions close to the rotors. The rubber compound close to the rotors just rotate with the rotors. The high values of mixing index ($0.8 < \lambda_{MZ} \leq 1.0$) was found in the

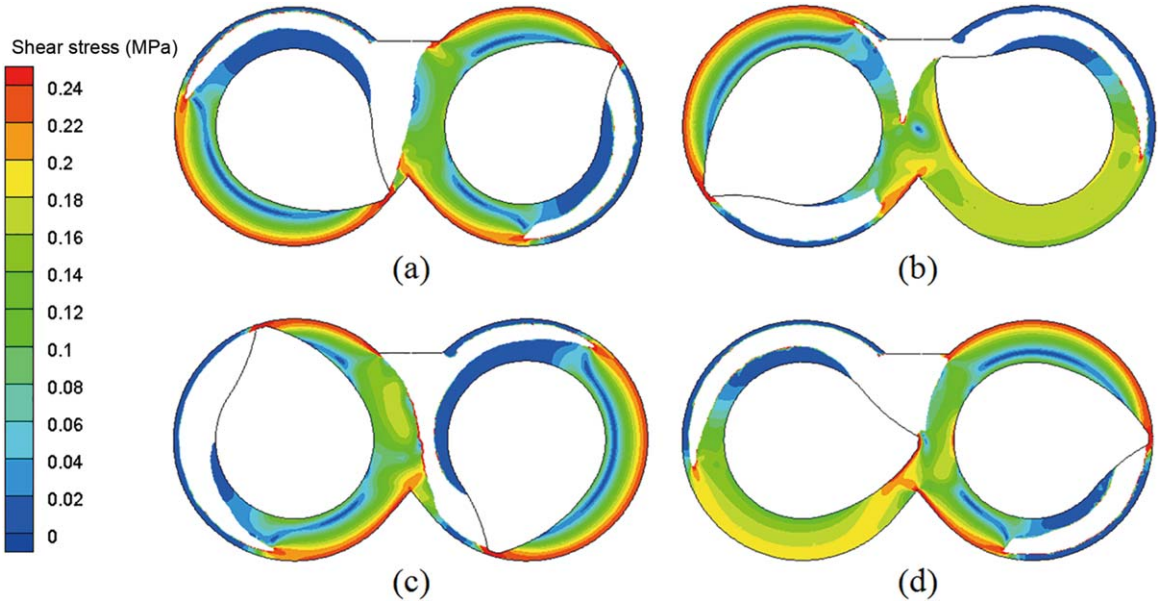

Figure 8. Shear stress distribution at four sequential locations of the rotors in a cycle: (a) $\theta = 36°$, (b) $\theta = 144°$, (c) $\theta = 252°$, and (d) $\theta = 360°$. [Color figure can be viewed in the online issue, which is available at wileyonlinelibrary.com.]

Table I. Average Values for Various Flow Characteristics in a Complete Cycle

Time (s)	Geometries	$\bar{\lambda}_{MZ}$	$\bar{\tau}$ (MPa)	$\bar{\dot{\gamma}}$ (1/s)
5.1	$\theta = 36°$	0.4140	0.10011	16.709
5.2	72°	0.4483	0.10487	16.180
5.3	108°	0.4061	0.10125	16.245
5.4	144°	0.5214	0.12254	15.042
5.5	180°	0.5013	0.11691	15.419
5.6	216°	0.4145	0.10076	16.641
5.7	252°	0.4367	0.10274	16.920
5.8	288°	0.4262	0.10103	15.854
5.9	324°	0.5258	0.12269	15.033
6.0	360°	0.5003	0.11981	16.004

middle of the flow channel due to the shrinkage of the flow channel. Although the elongational flow, which is advantageous to disperse dominates in the middle of the flow channel, the dispersive effect in such regions is not strong because the overall stress of the regions is relatively small. The region near the wall of the mixing chamber is mainly dominated by simple shear flow ($\lambda_{MZ} = 0.5$). The most region of the flow field is dominated by shear flow ($0.4 < \lambda_{MZ} \leq 0.6$).

From the volume distribution of mixing index (Figure 7), we can conclude that shear flow ($0.4 < \lambda_{MZ} < 0.6$) dominates in most of the flow region. In addition, there is a relatively large volume percentage of rubber compound experiencing rotational flow ($\lambda_{MZ} < 0.2$), and 50.05% of the rubber compound experiences better than simple shear flow ($\lambda_{MZ} > 0.5$).

Apart from elongation stress, shear stress is also related to dispersive mixing, and the higher the shear stress the higher the dispersion of the filler. Figure 8 shows the shear stress distribution at four sequential locations of the rotors in a cycle. The shear stress is high in the gap between the rotor blade tip and the chamber wall; that is, the rotor tip region is a main place for the filler to disperse. Another high shear zone is located near the chamber wall. The region behind the rotor tip has low shear stresses, with low or even no dispersive effect.

Comparing the distributions of mixing index and shear stress, we can see that the shear stresses are relatively low (<0.02 MPa) in the region where the mixing index is a minimum. The flow is mainly dominated by simple shear flow in the region where the shear stresses are relative high (>0.22 MPa).

From the volume distribution of shear stress (Figure 9), it can be clearly seen that shear stresses lower than 0.03 MPa occupy a high volume percentage because the shear stress of the rubber compound adhering to the rotors is low. The rotor design must ensure that the rubber compound in the low shear stress region can flow into the high shear region; otherwise, the mixing of the rubber compounds must be poor.

Table I shows the volume-weighted average values of the mixing index for the rubber compound, the shear stresses, and the shear rates in a complete cycle. As the rotors rotate in a cycle, the relative difference between the maximum and minimum values is 25.9, 22.4, and 11% for the mixing index, the shear stress, and the shear rate, respectively. This result indicates that there are large fluctuations of the mixing index, the shear stress, and the shear rate as the rotors rotate.

CONCLUSION

The main contribution of the article is that the rubber compound distributions, the flow parameters such as flow velocity and pressure in a partially filled internal mixer are obtained by simulation. This work can provide an improved understanding on the transient behaviors of flow patterns within an internal mixer, and deep understanding of the flow behaviors and mixing processes within an internal mixer is essential for its design, optimization, and scaling up.

Based on the simulation results, the following specific conclusions can be drawn:

1. After the flow has reached steady state, rubber compounds always distribute in the regions in front of the rotor blades and the gap regions between the rotors blades and inner wall of the mixing chamber. At the back of the rotor blades, no rubber compounds exist (Figure 3).
2. In the bridge region between the two rotors, there is exchange of material between the left and the right mixing chamber. Furthermore, the exchange of material is more violent with the rotor tip inside the bridge region rather than outside the bridge region.
3. The rotor blade tip region is a high shear zone and is a main place for the fillers to disperse. Kneading effect on the rubber compounds exists in the region near the blade tip corner.

ACKNOWLEDGMENTS

We acknowledge financial supports from the National Basic Research Program of China (2015CB654705), National Natural Science Foundation of China (51173016), Foundation for Innovative Research Groups of the National Natural Science Foundation of China (51221002), and National Natural Science Foundation of China Major International Joint Research Project (51320105012).

REFERENCES

1. Manas-Zloczower, I. *Rubber Chem. Technol.* **1994**, *67*, 504.
2. Campanelli, J. R.; Gurer, C.; Rose, T. L.; Varner, J. E. *Polym. Eng. Sci.* **2004**, *44*, 1247.
3. Nakajima, N. *Polym. Int.* **1996**, *41*, 23.
4. Toh, M.; Gondoh, T.; Mori, T.; Mishima, M. *J. Appl. Polym. Sci.* **2005**, *95*, 166.
5. Koolhiran, C.; White, J. L. *J. Appl. Polym. Sci.* **2000**, *78*, 1551.
6. Freakley, P. K.; Patel, S. R. *Rubber Chem. Technol.* **1985**, *58*, 751.
7. Freakley, P. K.; Idris, W. Y. W. *Rubber Chem. Technol.* **1979**, *52*, 134.
8. Min, K.; White, J. K. *Rubber Chem. Technol.* **1985**, *58*, 1024.

9. Min, K.; White, J. L. *Rubber Chem. Technol.* **1987**, *60*, 361.
10. Bai, Y.; Sundararaj, U. *AlChE J.* **2011**, *57*, 2657.
11. Wang, W.; Manas-Zloczower, I. *Polym. Eng. Sci.* **2001**, *41*, 1068.
12. Emin, M. A.; Schuchmann, H. P. *J. Food Eng.* **2013**, *115*, 132.
13. Ishikawa, T.; Kihara, S. I.; Funatsu, K. *Polym. Eng. Sci.* **2000**, *40*, 357.
14. Salahudeen, S. A.; Elleithy, R. H.; AlOthman, O.; AlZahrani, S. M. *Chem. Eng. Sci.* **2011**, *66*, 2502.
15. Zhou, J.; Yu, W.; Zhou, C. X. *J. Polym. Eng.* **2008**, *28*, 385.
16. Rathod, M. L.; Kokini, J. L. *J. Food Eng.* **2013**, *118*, 256.
17. Breuer, O.; Chen, H. B.; Lin, B.; Sundararaj, U. *J. Appl. Polym. Sci.* **2005**, *97*, 136.
18. Ghoreishy, M. H. R.; Nassehi, V. *Adv. Polym. Tech.* **1997**, *16*, 45.
19. Connelly, R. K.; Kokini, J. L. *Adv. Polym. Tech.* **2006**, *25*, 182.
20. Connelly, R. K.; Kokini, J. L. *AlChE J.* **2006**, *52*, 3383.
21. Zhang, X. M.; Feng, L. F.; Chen, W. X.; Hu, G. H. *Polym. Eng. Sci.* **2009**, *49*, 1772.
22. Bravo, V. L.; Hrymak, A. N.; Wright, A. N. *Polym. Eng. Sci.* **2000**, *40*, 525.
23. Connelly, R. K.; Kokini, J. L. *J. Food Eng.* **2007**, *79*, 956.
24. Nassehi, V.; Ghoreishy, M. H. R. *Int. Polym. Proc.* **1998**, *13*, 231.
25. Nassehi, V.; Ghoreishy, M. H. R. *Adv. Polym. Technol.* **2001**, *20*, 132.
26. Devals, C.; Heniche, M.; Bertrand, F.; Tanguy, P. A.; Hayes, R. E. *Int. J. Numer. Methods Fluids* **2007**, *53*, 735.
27. Hanspal, N. S.; Nassehi, V.; Ghoreishy, M. H. R. *Int. Polym. Proc.* **2005**, *120*, 238.
28. Shin, S.; Il, L. W. *Int. J. Heat Fluid Flow* **2000**, *21*, 197.
29. Rodrigo, J. G. L.; Rosa, M. Q. F. *Ind. Eng. Chem. Res.* **2009**, *48*, 1740.
30. Yuwen, X. X.; Chen, L.; Han, Y. J. *Energy Proc.* **2012**, *17*, 1864.
31. Shi, X.; Xiang, Y.; Wen, L. X.; Chen, J. F. *Chem. Eng. J.* **2013**, *228*, 1040.
32. Jeon, S. S.; Kim, S. J.; Park, G. C. *Chem. Eng. Sci.* **2011**, *66*, 5899.
33. Gopala, V. R.; Wachem, B. G. M. *Chem. Eng. J.* **2008**, *141*, 204.
34. Marsooli, R.; Wu, W. *Adv. Water Resour.* **2014**, *70*, 104.
35. Mu, Z.; Zhang, Z.; Zhao, T. *Proc. Eng.* **2012**, *28*, 808.
36. Cross, M. M. *J. Colloid Sci.* **1965**, *20*, 417.
37. Hirt, C. W.; Nichols, B. D. *J. Comput. Phys.* **1981**, *39*, 201.
38. Petera, J.; Nassehi, V. *Int. J. Numer. Methods Fluids* **1996**, *23*, 1117.
39. Cheng, J. J.; Manas-Zloczower, I. *Int. Polym. Proc.* **1990**, *5*, 178.